Phonon-imaging Measurement of Group Velocities and Elastic Constants in $CaWO_4$

Timothy L. Head[1,*] and Madeleine E. Msall[2]

[1]*Department of Physics, Abilene Christian University, Abilene, Texas, USA*
[2]*Department of Physics and Astronomy, Bowdoin College, Brunswick, Maine, USA*

(Received April 11, 2010)

The CRESST dark matter search employs phonon-mediated detectors with $CaWO_4$ absorbers, prompting renewed interest in its thermal properties. We use phonon-imaging techniques to measure temporal and spatial phonon flux distributions in a [001]-oriented $CaWO_4$ crystal. Data from the crystal and simulations based on continuum elasticity theory are used to calculate values of the elastic constants. The measured elastic constant values are consistent with those measured previously by Farley *et al.* via ultrasonic pulses, except for C_{13} and C_{16}, which differ by 15% and 8%, respectively.

PACS numbers: 63.20.de; 66.70.-f; 62.30.+d;81.40.Jj

I. OVERVIEW AND MOTIVATION

A current dark matter search known as the Cryogenic Rare Event Search with Superconducting Thermometers (CRESST) has chosen $CaWO_4$ as the absorber material for the detection apparatus [1]. Because the method used for distinguishing dark-matter events from background sources relies on the determination of the ratio of energy deposited in the absorber as light to that deposited as vibration, accurate calibration of energy deposition in the vibrational energy absorption channel is essential for event discrimination. This calibration will require detailed knowledge of the spatial and temporal evolution of the deposited thermal energy, which is strongly influenced by the values of the elastic constants of the absorber material.

An initial heat pulse experiment in $CaWO_4$ measured the non-equilibrium phonon flux along a single crystalline direction and found some discrepancies with previously measured elastic constant values as well as an unexplained non-linear phonon signal arriving between longitudinal acoustic (LA) and transverse acoustic (TA) phonon modes [2]. We employ the phonon-imaging technique to map the non-equilibrium phonon flux through [001]-oriented $CaWO_4$ single crystals for a wide range of propagation directions. These measurements provide phonon group velocities for each propagation direction. Our experiments use group velocities along high-symmetry directions to directly measure some elastic constant values, and an indirect method of comparing simulated and experimental images to measure all the seven elastic constants.

Ultrasound experiments assume planar excitation and phonon propagation described by the phase velocity. By contrast, phonon-imaging uses point excitations where phonon

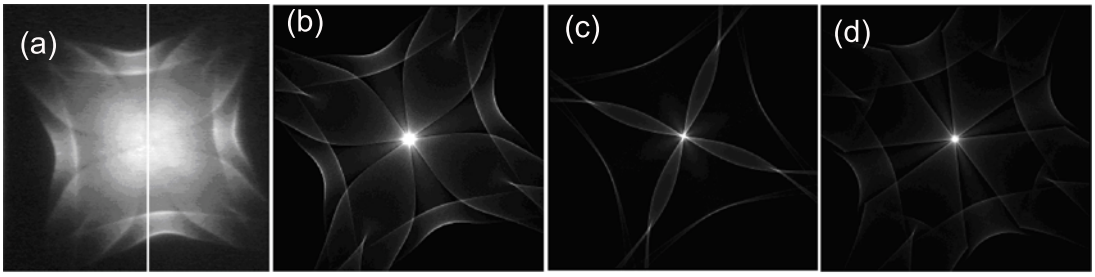

FIG. 1: Phonon images through 2.8 mm [001]-oriented $CaWO_4$ (image faces are 8.4 mm squares). (a) Experimental image. The bright spot at the center of the cross structure corresponds to the (001) propagation direction. The vertical line corresponds to data in Fig. 3. (b) Best-fit simulated phonon image using the following elastic constants (in GPa): $C_{11} = 51.5$, $C_{12} = 65.54$, $C_{13} = 47.42$, $C_{16} = -18.81$, $C_{33} = 134.04$, $C_{44} = 35.39$, and $C_{66} = 39.6$; the value of ρ used was 6120 kg/m^3. (c) Simulated image using the constants of Gluyas *et al.* [5]. (d) Simulated image using the constants of Farley *et al.* [4].

propagation is described by the group velocity. Because crystals are not isotropic, many phonons with differing wavevectors may move along the same group velocity direction [3]. This effect causes an isotropic momentum distribution, resulting in an anisotropic group velocity distribution in the crystal. A further consequence is phonon focusing, where the anisotropic propagation concentrates energy along certain directions [3].

Phonon-imaging experiments map out non-equilibrium phonon flux as a function of the propagation direction by scanning a laser across the crystal face and detecting the resulting phonon flux on the other side. The experiments are performed at temperatures near 2 K to decrease scattering between phonons generated by the heat source and thermal phonons and to accommodate the use of superconducting bolometers as phonon detectors. The resulting map of the phonon intensity as a function of the laser position is known as a phonon image. The phonon images (see Fig. 1(a)) show abrupt transitions between bright areas of high phonon flux and dark areas of low phonon flux, known as caustic lines. The positions of caustic lines are directly related to folds at the group-velocity surface and are particularly sensitive to the values of the elastic constants.

The present work uses the sensitivity of the caustic line positions to the variation of the elastic constants as a tool to determine appropriate low-temperature elastic constants of $CaWO_4$. We do this by comparing continuum-limit, time-integrated Monte-Carlo simulations to experimental phonon images and adjusting the elastic constants input into the simulation to best match the measured images. We compare our values with those measured previously in ultrasonic measurements [4, 5].

The phonon-imaging technique also allows experimental access to the arrival times of phonons. Using the ballistic time of flight and laser position, we can directly calculate the phonon group-velocity surfaces, which are very useful in identifying phonon modes.

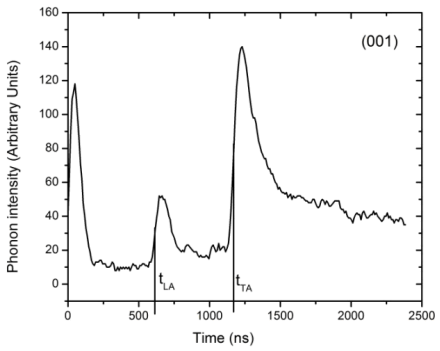

FIG. 2: Time trace of phonon intensity through 2.8 mm of $CaWO_4$ at the (001) point in Fig. 1(a). The initial pulse is the direct excitation of the detector by scattered laser light. The times $t_{LA} = 613$ ns and $t_{TA} = 1170$ ns correspond to the arrival of the longitudinal and transverse acoustic waves along this direction.

II. EXPERIMENTAL DETAILS

This paper reports on phonon-imaging results for a [001]-oriented $CaWO_4$ crystal with a thickness of 2.8 mm and a 20 mm^2 face. The sample is prepared by depositing a 150 nm copper film on the excitation surface to absorb laser light and provide a Planckian phonon source [6]. An $Al_{2-x}O_x$ bolometer deposited on the opposite face serves as a phonon detector. The detector is photolithographically patterned and has an active area of $\sim 5 \times 10$ μm^2 and a sharp superconducting transition below 1.7 K. The phonon source is a 20 ns pulsed Ar-ion laser with a repetition rate of 10–20 kHz and a Gaussian beam width of ~ 10 μm at the sample. The laser is scanned across the excitation surface and the signal level is recorded at each position to construct a map of phonon flux vs. phonon propagation direction. The sample is immersed in a liquid helium bath to maintain the detector temperature just below its superconducting transition. The detector is then current biased to maximize the signal-to-noise ratio while minimizing the physical size of the detecting region.

The spatial resolution of the experiment is given by the convolution of the source and detector sizes, but can also be significantly affected by phonon scattering in the sample. We measure the effective spatial resolution by scanning the laser across a target affixed to the sample surface. The target consists of a series of reflective lines that obscure the incoming laser light, producing a superimposed image of the target on the phonon image. The 10–90% rise distance across a sharp edge on the target is 72 μm, which corresponds to a Gaussian width of 32.8 μm. The phonon images were collected in arrays with a spacing of 32.8 μm.

A typical laser excitation pulse contains approximately 1 μJ of energy, which corresponds to an average laser power of about 40 mW. Assuming 30% beam loss from the final optical elements and another 40% reflected by the copper film, the irradiance absorbed by

the copper film is typically 50 W/mm^2. We calculate the phonon source temperature by ignoring the acoustic mismatch and assuming that 40% of phonons travel from the copper to the liquid helium. Given this assumption, the Stefan-Boltzman constant from copper to helium is $\sigma_{\mathrm{Cu/He}} = 444$ W/m^2 K^4. Calculations of emissivity between disordered metal films and dielectric substrates suggest that the emissivity at a copper – helium interface should be about half the value of emissivity at the copper – sample interface. Using these estimates, our phonon source may reach temperatures as high as 100 K.

Although this is a very high source temperature, the phonon source is also short lived, as may be seen by the fast disappearance of the phonon signal in Figure 2. This rapid cooling is due to direct contact of the excitation surface with the superfluid helium bath. The phonon signals show larger tails in the temporal distributions at higher excitation powers, suggesting an increase in isotope and anharmonic phonon scattering because of the phonon source producing more high-frequency phonons with a higher temperature Planckian source. Figure 2 shows the temporal distribution of phonon flux measured for phonon propagation along the (001) direction, which corresponds to the brightest spot in Fig. 1(a). The initial pulse of the distribution is the reaction of the detector to scattered laser light, and it marks the time t = 0 in the experiment. We also use this pulse to ascertain the temporal response of the detector by noting that the full width at half-maximum is 95 ns and the 10–90% rise time of the pulse is 51 ns. Temporal data was collected at 10 ns intervals, which limited our time resolution.

III. GROUP VELOCITY MEASUREMENTS

Experimentally, phonon imaging yields group velocity values when we monitor the phonon arrival times in time traces similar to that shown in Fig. 2. From the laser position, we calculate the phonon path length. The phonon mode arrival time is found by recording the midpoint of the rise and subtracting 25 ns to account for the width of the detector response. Figure 3(a) shows a plot of phonon intensity variation as a function of time (horizontal axis) and laser position along the vertical line through the (001) point in Fig. 1(a) (vertical axis). Each of the laser positions in the figure yields a set of group velocities along that direction. Figure 3(b) shows the calculated group velocities along the vertical line through the (001) point in Fig. 1(a).

Once measured, we correlate the group velocities with the seven independent elastic constants of the scheelite-structured $CaWO_4$ in one of two ways. First, along some symmetry directions, the group velocity and phase velocity are equivalent, and there is an analytic relationship between the group velocity and some elastic constants in these directions. The phase velocities and polarizations are the solutions to the Christoffel equation for the crystal, and the group velocity is related to the polarization **e** and wavevector **k** by

$$V_n = \frac{\partial \omega}{\partial k} = \frac{e_i \, C_{ijln} k_j e_l}{\rho \, \omega}. \tag{1}$$

Here, ω is the angular frequency, ρ is the density, and C_{ijln} is the fourth-rank elastic stiffness

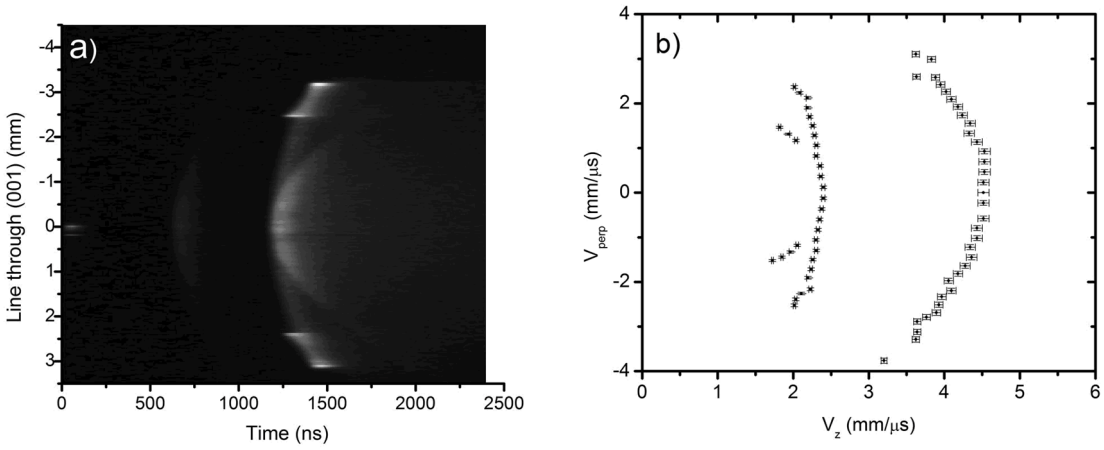

FIG. 3: (a) Position vs. time plot of phonon intensities along the center scan line shown in Fig. 1(a) ([001]-oriented sample). (b) Group velocities calculated from the arrival times shown in part (a).

tensor. Summation notation over repeated indices is assumed, and we will use the condensed Voigt notation to describe the elastic constants in the rest of the paper. Unfortunately, the wavevectors and polarizations are not experimentally accessible to us, except along symmetry directions where the vibrational polarization modes are purely longitudinal or transverse and so group velocity and phase velocities are equivalent. For instance, some phonon modes traveling along the (001) direction can be identified as having a purely longitudinal or purely transverse polarization, simplifying the relationship between the measured velocity and elastic constants to

$$\nu_{LA} = \sqrt{\frac{C_{33}}{\rho}} \text{ and } \nu_{TA} = \sqrt{\frac{C_{44}}{\rho}}. \tag{2}$$

From the arrival times in Fig. 2, we calculate the group velocities $\nu_{LA} = 4.76 \pm .08$ mm/μs and $\nu_{TA} = 2.45 \pm .02$ mm/μs along the (001) direction, allowing the calculation of both $C_{33} = 138 \pm 5$ and $C_{44} = 36.6 \pm 0.7$ GPa with $\rho = 6120$ kg/m^3. We do not compensate for the temperature dependence of the density, but preliminary calculation shows that the correction to the elastic constants would be significantly less than our uncertainty in the measurement.

Second, we determine the remaining elastic constants (as well as the two we have measured directly) by comparison of experimental phonon images with phonon images generated in a Monte-Carlo simulation based on continuum elasticity theory. The simulation requires the phonon density, sample dimensions, and the seven elastic constants as inputs; uses these values to calculate group velocities; and then generates a phonon image by using an isotropic momentum distribution. We compare the simulated image to the experimental one, adjust the elastic constants, and iterate until we have good agreement between the simulated and experimental images. We are currently working on an automated fitting

routine, but the seven free parameters and a highly non-linear function make global fitting a difficult proposition [7]. In the meantime, we have made significant progress by comparing images by eye.

TABLE I: Measured elastic constant values of $CaWO_4$.

Elastic Constants (GPa)	Farley *et al.*[a] (1.5 K)	Gluyas *et al.*[b] (4.2 K)	Current Work Direct Measurement	Current Work Image Analysis
C_{11}	152.3	150.6		151 ± 3
C_{12}	65.27	65.89		66 ± 3
C_{13}	40.78	58.94		47 ± 2
C_{16}	20.37	17.21		19 ± 1
C_{33}	132.4	135.6	138 ± 5	134 ± 3
C_{44}	35.0	35.75	36.6 ± 0.7	35.4 ± 0.7
C_{66}	40.31	47.74		40 ± 2

[a]Reference [4].
[b]Reference [5].

Using this procedure, we find the values of the elastic constants to be somewhat close to those of Farley *et al.* [4]. The closest matching simulation images occur for values near the average of the elastic constant values measured by Farley and Gluyas [4, 5]. Our values are listed in Table I.

During analysis, we found that the data image in Fig. 1(a) seemed to be rotated significantly compared to our simulations. While adjusting the elastic constants could account for some rotation around the fourfold axis, we could not account for the magnitude of rotation that we observed. We tested for the orientation of the [010] axis with respect to the crystal edges using electron backscatter diffraction and found that the [010] axis is rotated by $17^\circ \pm 1/2^\circ$ with respect to the edge of our sample. Allowing for this rotation was essential for extracting elastic constants from the image data. Figure 1(a) shows the raw data uncorrected for this rotation.

IV. DISCUSSION

Phonon imaging has been used to identify the elastic constants of $CaWO_4$. Direct measurements of C_{33} and C_{44} yield values that agree with previous measurements [4, 5]. The direct measurements of C_{33} and C_{44} are limited by the uncertainty in the ballistic arrival time of phonons at the detector. The uncertainty is approximately 10 ns and is due to the size of the time step used during data collection. We chose to use the midpoint of the rise in our calculations to avoid uncertainty in the precise time that the signal overcomes the noise. This required a 25 ns correction to avoid a systematic offset in the arrival time. The resulting uncertainty in our direct measurements of C_{33} and C_{44} is somewhat larger than the measurements made by the ultrasonic method, where multiple reflections of the

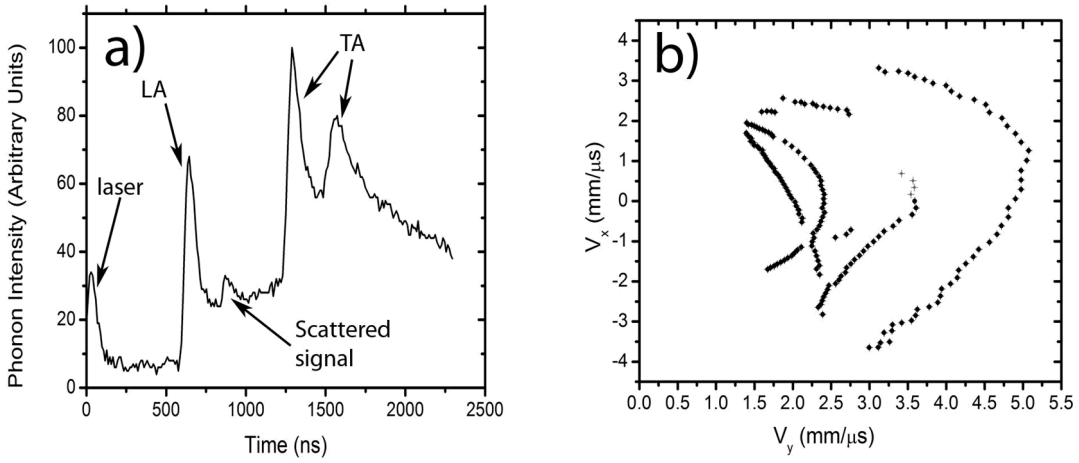

FIG. 4: Data from a 3.0 mm thick [010]-oriented $CaWO_4$ sample. More detailed information and discussion of data from this sample are available in reference [7]. (a) Time trace of phonons arriving just above the (010) direction and (b) group velocities calculated from phonon arrival along the line $z = 0$ (the V_z component of the group velocity is zero). The lighter points just above the (010) point are likely to be phonons that have undergone small-angle scattering from the caustic direction, as suggested by Hayasaka *et al.* [2].

ultrasonic pulses were used to decrease the uncertainty in the measurement.

Phonon imaging really comes into its own using the image comparison technique to find an entire set of elastic constants. The differences between the elastic constants measured by Gluyas and Farley make obvious changes in the caustic shapes and positions, as seen in Fig. 1. By matching the experimental images with simulations, we can hone in on the whole set of elastic constants.

The main discrepancy between the two sets of previously measured ultrasonic data is a difference of 35% in the values of C_{13} and differences of $\sim 15\%$ in C_{16} and C_{66}. Thus, we concentrate on improving these, allowing only small variations in the other elastic constants for which there is good agreement. The caustic positions of the central cross pattern in Fig. 1(a) are very sensitive to the value of C_{13}. The shapes of the same caustics are also sensitive to the values of C_{16} and C_{66}. For these particular caustic regions, we find that the values of the elastic constants shown in Table I best reproduce the experimental images. Figures 1(a) and (b) show the experimental data and best-fit image side by side. Note that the axis rotation is not taken into account in these comparisons. Using this method, the uncertainty in the elastic constant values is within 2%.

Earlier heat pulse measurements found an anomalous phonon mode very near to the (010) propagation direction with highly non-linear power dependence [2]. We observe no unusual power dependences in our measurements. However, measurements on a second $CaWO_4$ sample oriented with a [010] face have shown a small "extra" phonon peak for phonons traveling *near* the (010) direction [8]. Figure 4(a) shows a time trace of such a

phonon pulse, and Fig. 4(b) shows a slice of the measured group velocity surface for the [010]-oriented sample along the z = 0 line. The group velocities of the extra peak shown in Fig. 4(b) are denoted by the lighter points just above the (010) direction. Ballistic phonons are not predicted to travel along these directions, but the existence of this peak is probably due to channeling of phonons scattered through small angles from the nearby caustic direction, as discussed by Hayasaka *et al.* [2].

V. CONCLUSIONS

The sensitivity of the phonon caustic shape and position to small changes in the elastic constants has been exploited to determine more precise values of the elastic constants of $CaWO_4$, particularly C_{13}, C_{16}, and C_{66}. The elastic constants C_{33} and C_{44} have also been measured directly. These values are in good agreement with previous measurements [4, 5]. We have also observed a pulse of scattered phonons that seems to correspond to the previously observed "anomalous mode." However, we did not observe the nonlinear power dependence of its amplitude.

Work is underway to numerically analyze phonon images, but the problem is complicated by highly nonlinear intensity variations within images and a large number of fitting parameters. Precise knowledge of the elastic constants and non-equilibrium thermal evolution of this material is important for accurate modeling with high-precision calorimetric measurements, such as those undertaken by CRESST in the search for dark matter.

Acknowledgments

The authors give many thanks to Keith Wigmore and Shin Tamura for their encouragement and to Hans Kraus and Vitaly Mihalik for beautiful samples. We also wish to acknowledge J. P. Wolfe and the Frederick Seitz Materials Research Lab for use of facilities, and partial support of this research project as well as the Abilene Christian Math/Science Grant and Bowdoin College for support. Helpful contributions were also made by Rachel Beane, Daniel Jumper, and Nat McConnell.

References

* Electronic address: tim.head@acu.edu

[1] R. F. Lang, and W. Seidel, New Journal of Physics. **11**, 105017(2009).
[2] K. Hayasaka, R. Higashi, J. Suda, Y. Tanaka, S. Tamura, M. Giltrow, and J. K. Wigmore, Solid State Communications **143**, 386 (2007).
[3] J. P. Wolfe, *Imaging Phonons*, (Cambridge University Press, New York, 1998).
[4] J. M. Farley, and G. A. Saunders, J. Phys. C **5**, 3021 (1972).
[5] M. Gluyas, F. D. Hughes, and B. W. James, J. Phys. D **6**, 2025 (1973).
[6] O. Weis, Z. Angew. Physik B **80**, 15 (1990).
[7] M. Msall and T. L. Head, Submitted to Chinese Journal of Physics (2010).
[8] M. E. Msall, D. S. Jumper, and T. L. Head, Submitted to Solid State Communications (2010).